Paper presented at the 22nd Asian Conference on Remote Sensing, 5 - 9 November 2001, Singapore.

QUALITY ANALYSIS ON HEIGHT DISPLACEMENT VALUES DETERMINED BY THREE-PASS METHOD AND SOME TEST RESULTS IN URBAN AREA IN TAIWAN

Jaan-Rong TSAY[1] and Chien-Hsian Lu [2]
Assistant Professor[1] and graduate student [2], Department of Surveying Engineering
National Cheng Kung University
1, University Road, 70101 Tainan
Tel: (886)-6-237-0876 ext. 838 Fax: (886)-6-237-5764
E-mail: tsayjr@mail.ncku.edu.tw
TAIWAN, R.O.C.

KEY WORDS: Three-pass method, INSAR, CEOS, SLC, DDM

ABSTRACT: Three-pass method utilizes ERS data to create DDMs in Taiwan. Some basic theoretic aspects are firstly analyzed. It verifies that INSAR can provide a DDM with an accuracy of a few millimeters, if INSAR can creates a DEM with an accuracy of a few meters. Comparing with the precise displacements determined using GPS shows that the mean difference of the displacement values estimated by D-INSAR and the ones determined by GPS is about 6cm. It indicates that three-pass method and ERS data processed properly can detect height surface deformation in urban area in Taiwan.

1. INTRODUCTION

Radar (=RAdio Detection And Ranging) is an active sensor, transmitting a signal of electromagnetic energy, illuminating the terrain, and recording or measuring the response returned from the target or surface. Its weather independence and 24-hour operation capabilities are the two most widely touted and valuable characteristics. SAR (=Synthetic Aperture Radar) is a radar technique, in which an artificially long antenna can be synthetically created using a transported small antenna. It permits fine resolution in the azimuth direction (along flight path) using longer radar wavelength (Henderson & Lewis, 1998). SAR not only obtains the radar scattering coefficient of the land cover, but also carries the phase information about the target when a pair of data is coherently processed. D-INSAR (=Differential Interferometric SAR) is a SAR technique and uses the differential interferogram in the same area but at different time to calculate surface deformation. It can determine an abrupt height change (e.g. due to earthquake or landslide) and a slow gradual height change (e.g. due to land subsidence or slow crustal movement). The three-pass method is one of D-INSAR techniques. In this paper, the computation steps of three-pass method will be described. The quality of its output products is to be analyzed in a basic manner. Some test results in urban area in Taiwan will be presented briefly.

2. THREE-PASS METHOD

Two subsystems of the Vexcels 3DSAR SAR processing system package are used in our tests. They are called FOCUS and PHASE. The algorithm and parameters adopted in our tests and for our test data are described briefly as follows. For detail please see (Vexcel, 2000).

2.1 FOCUS – SAR processor

FOCUS is the name of Vexcels SAR processor. It consists of three subsystems: ①SAR Parameter Estimation, ② range Doppler algorithm, and ③ CEOS (=Committee on Earth Observation Satellites) conversion. The well-known range Doppler algorithm is used to focus the input raw SAR data (phase history data) in the so-called CEOS L0 format. Parameter Estimation utilizes two algorithms, MLBF (multi-look beat frequency) and MLCC (multi-look cross correlation), to figure out the Doppler ambiguity number. MLBF and MLCC work best for high- and low-contrast scenes, respectively. Both algorithms are performed at different parts of the image and the best consistent result for the ambiguity number is selected. The Correlation Doppler Estimator (CDE) or the Sign Doppler Estimator (SDE) is chosen by the field Doppler Estimator to estimate the ambiguous part of the Doppler centroid. The Doppler rate is determined using the range correlation algorithm. The SAR parameters obtained in Parameter Estimation are basically the *Doppler centroid* and *Doppler rate*. Both are needed to determine the azimuth chirp function used in the azimuth compression. They are then used to set up two 1D Fast Fourier Transforms (FFT). Firstly, range compression is performed through multiplying the input raw range lines with the range chirp, where the range chirp coefficients are determined by the sensor/beam characteristics of the satellite. Azimuth compression is then done using the azimuth chirp coefficients obtained earlier. In addition, range curvature correction with secondary range migration,

radiometric calibration, multi-looking, and resampling to ground range might be performed. Finally, FOCUS produces standard CEOS L1 datasets, e.g. CEOS SLC (single-look complex image) data for ERS1/2 used in our tests.

2.2 Three-Pass Method

A digital displacement model (DDM) can be generated using three different SLC images (passes). Since it utilizes three passes as the main input data, it is called 'three-pass method'. It is a subsystem of PHASE, which is a complete SAR interferometry processing system. The subsystem assumes that the displacement is due either to an abrupt displacement or else a displacement that is uniform in time. If the abrupt model is used, the passes should be chosen in such a way that an event causing displacement occurs between the reference SLC and the third SLC, but does not occur between the reference SLC and the second SLC. Moreover, an interferogram is an image created by taking one SLC and then multiplying it by the complex conjugate of a second. The resolution is usually reduced by multi-looking. The phase of the so-called reference interferogram, which is the interferogram formed between the reference SLC and the second SLC, reflects the topography of the scene and so it can be subtracted from the phase of the second interferogram, which is the interferogram formed between the reference SLC and the third SLC, leaving only the phase due to ground displacement caused by the event. Furthermore, each pixel of an SLC has a satellite position associated with it. When an interferogram is created, each pixel of the interferogram has a baseline representing the distance between the satellite positions associated with the two corresponding SLC pixels.

In the three-pass method, a displacement map is generated using three SLCs as follows: 1. Resample the second SLC to the geometry of the reference SLC, 2. Create the reference interferogram between the reference SLC and the second SLC, 3. Filter the reference interferogram, 4. Unwrap the reference interferogram, 5. Refine the geometry of the reference interferogram by using GCPs (ground control points), 6. Resample the third SLC into the geometry of the reference SLC, 7. Create the second interferogram between the reference SLC and the third SLC, 8. Flatten the second interferogram by subtracting the unwrapped phase of the reference interferogram, 9. Filter the flattened interferogram, 10. Unwrap the flattened interferogram, 11. Refine the baseline of the second interferogram, 12. Create the displacement map.

The steps 1-7 and 9-10 are described in (Tsay and Chen, 2001). In the step 8, the simulated phase is recalculated using the refined baseline and then subtracted from the unwrapped interferogram. The flattened interferogram should be corrupted less by filtering and more amenable to phase unwrapping. If the phase is simulated with the estimated baseline rather than the refined exact baseline, there may be a residual phase ramp in the interferogram and there may also be some residual topographic signal remaining. In the step 11, the simulated phase is also recalculated from the refined baseline and subtracted from the interferogram to form the refined interferogram. The refined interferogram is not used in any subsequent processing, it is merely computed so that one can determine whether the refined baseline is successful in removing topographic signal. If the topographic signal is not completely removed, it is suggested to remove bad GCPs and compute the refined baseline again. In particularly, it is recommended that GCPs are not used in regions where large displacements are observed. In the step 12, two displacement models are available: ①*abrupt change* – this model assumes that the displacement occurs between the reference SLC and the third SLC and no displacement occurs between the reference SLC and the second SLC, ② *continuous change* – this model assumes that the displacement rate is constant during the time spanned by all three SLCs.

In brief, two interferograms are created that have a common reference SLC. The reference interferogram has a phase that is just due to topography. The secondary interferogram has a phase due to both topography and ground motion, but the phase due to topography can be calculated from the reference interferogram and subtracted from the secondary interferogram. The phase due to ground motion can thus be estimated and also the DDM can be calculated.

3. ERROR SOURCES

For the present, many successful application examples are verified, but the SAR technique is not yet completely able to provide the surface change information at the level of confidence by seismology and geoscience communities. This is mainly due to several radiometric, geometric, and timing error sources such as (1) ***radar system***: ①timing and control, ② RF (Radio Frequency, analog) electronics, ③digital electronics and data routing, ④antenna (2) ***platform (spacecraft or aircraft) and data downlink system***: ①channel errors, ②downlink data rate reduction, ③data compression, ④block floating point quantization (3) ***ground data processing system***: ①correlator algorithms and architectures, ②radiometric correction, ③geometric correction, ④image data browse (Curlander & McDonough, 1991) and (4) ***model errors***: e.g. the discrepancy between theoretical assumptions and corresponding realities. For example, INSAR, like other astronomic and space geodetic techniques, is limited by the spatially and temporally

variable delay of electromagnetic waves propagating through the neutral atmosphere. The atmospheric conditions introduce the tropospheric delay to the total path delay and thus increase the level of uncertainties in the order of centimeter scale. Traveling ionospheric disturbance also contributes additional propagation delay (Zebker et al., 1997). Interferometry demands that the phase of a radar echo be reproducible. That is, if we measure the phases of the radar echoes from exactly the same place again, they should be identical. In reality, the phases may differ and thus cause some errors in all INSAR products. This phase difference is called decorrelation of the phase, and is measured by the *coherence* or correlation. The main factors that may cause decorrelation are ①temporal decorrelation, ②baseline decorrelation, and ③squint decorrelation. Squint decorrelation may be a problem if the difference in the Doppler frequencies of the two different acquisitions is not very small compared to the pulse repetition frequency. If the decorrelation becomes too large, the phase data cannot be unwrapped, and it becomes unusable.

4. QUALITY ANALYSIS

We assume a simple SAR geometry as shown in Figure 1. The three SLCs are S_1, S_2 and S_3, respectively. A ground point P moves to P′ between the two acquisitions S_1 and S_2. The three points S_1, P and P′ are assumed to lie on a straight line. One can derive the equations (1) and (2):

$$df \approx \frac{-4pB\cos(q-a)}{lR_1 \sin q} \cdot dh \tag{1}$$

$$df = \frac{4p}{l} \cdot d(dR) \tag{2}$$

For our test data, radar wavelength $\lambda \approx 0.057$m, baseline $B \approx 220$m, $R_1 \approx 785000$m, look angle $q \approx 23°$. Figure 2 shows the relationship between the phase error df and the height error dh at the point P and the one between df and the displacement error $d(dR)$ at the point P, respectively. In case of $a=0°$, a height error $dh=1$m will cause a phase error $df \approx -9°$, while a displacement error $d(dR)=1$m will cause a phase error $df \approx 12631°$. Therefore, INSAR can provide a DDM with an accuracy of a few millimeters, if INSAR can creates a DEM with an accuracy of a few meters (Zebker et al. 1994).

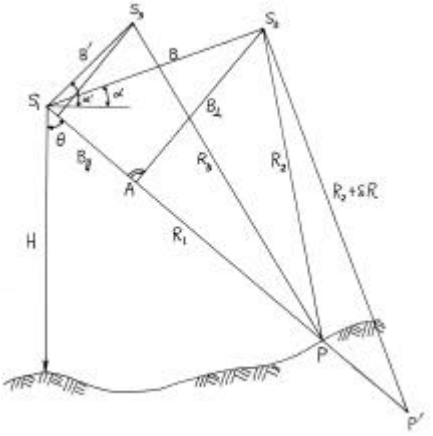

Figure 1. A Simplified Geometry of SAR Interferometry, ref. (Zhou et al., 1998), with $R_1 = R_2 + dR = R_3 + dR'$.

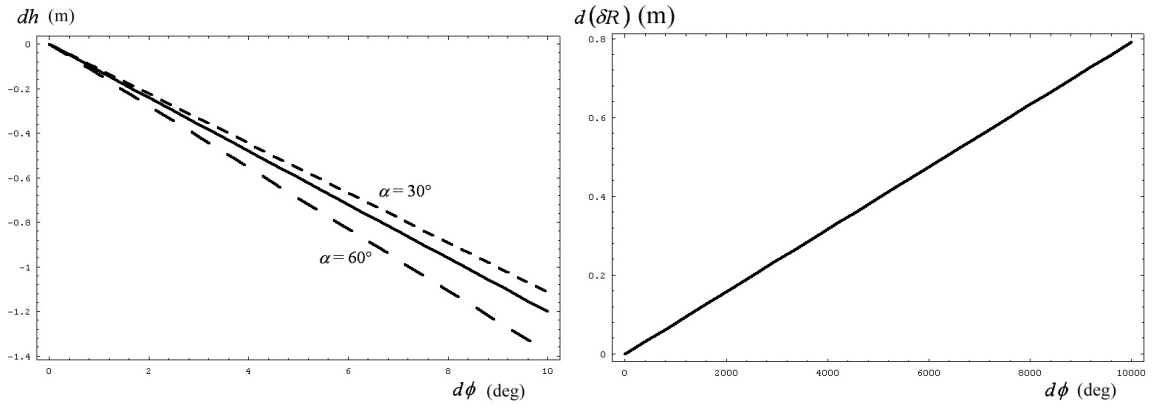

Figure 2. Relationship between the phase error df and the height error dh (left, the solid line denotes a=0°) and between df and the displacement error $d(dR)$ if ERS1/2 data in Taiwan is used.

5. TEST RESULTS

Four ERS-2 data in raw CEOS format from the track 232 and the frame 3123 are used in all tests. They cover the central Taiwan and are acquired on January 21, May 6, September 23, and October 28 in 1999, respectively. The test area is the urban area in central Taiwan near the epicenter of Chi-Chi earthquake that happened at 1:47 a.m. on September 21, 1999. The reference interferogram is formed from the two SLCs acquired on May 6, 1999 and January 21, 1999, respectively, which is before the earthquake. The secondary interferogram will be formed either from the two SLCs acquired on May 6, 1999 and September 23, 1999 or from the two SLCs acquired on May 6, 1999 and October 28, respectively. The earthquake occurred between the two passes that form the secondary interferogram, so the displacement will be estimated. Firstly, the "Estimate Baseline", "Resample secondary SLC" and "Create interferogram" processes are done. Table 1 shows some basic data of these three SLC pairs: their approximate perpendicular and parallel baselines, and registration results (number of tie points, SNR threshold, and the errors of the fit in the azimuth and range directions). Figure 3 shows their coherence images. The coherence is less than 0.2 in eastern mountain area. The urban area has a coherence c.a. in the range 0.5-0.7. The coherence is zero in the western ocean area. Figure 4 shows the three inteferograms. The third interferogram (May 06/Oct.28) has clearer fringes than the second one (May 06/Sep.23), because its coherence is larger as shown in Figure 3. The reference interfergram is clearest, since the other two ones contain at least the decorrelation caused by the Chi-chi earthquake.

Table 1. Three SLC pairs and their approximate perpendicular and parallel baselines, and registration results (number of tie points, SNR threshold, and the errors of the fit in the azimuth and range directions)

				Registration			
Ref. SLC	2nd SLC	per. BL (m)	par. BL (m)	no. of tie points	SNR threshold	azi. err. (pixels)	ran. err. (pixels)
May 06	Jan. 21	89	-89	570	11	0.127	0.101
May 06	Sep. 23	-206	49	167	12	0.290	0.150
May 06	Oct. 28	16	-41	107	12	0.212	0.071

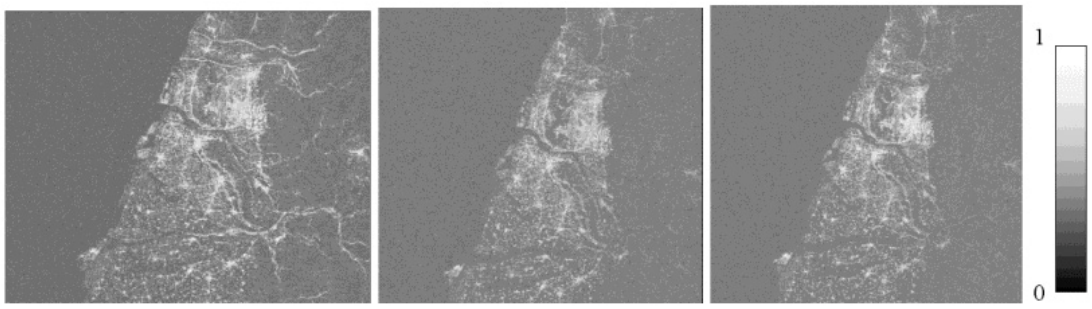

Figure 3. Three coherence images: May 06/Jan. 21 (left, $B_\perp \cong$97m), May 06/Sep. 23 (middle, $B_\perp \cong$-220m), May 06/Oct. 28 (right, $B_\perp \cong$5m), where $B_\perp$ denotes the perpendicular baseline.

igure 4. Three inteferograms: May 06/Jan. 21 (left, $B_\perp \cong$97m), May 06/Sep. 23 (middle, $B_\perp \cong$-220m), May 06/Oct. 28 (right, $B_\perp \cong$5m), where $B_\perp$ denotes the perpendicular baseline.

Now step through the "Filter reference", "Unwrap reference" and "Refine reference geometry" processes. Refine the geometry of the reference interferogram by using GCPs, whose positions are shown in Figure 5. The filtered, unwrapped, and refined reference interferograms are shown in Figure 6.

Then run through the, "resample third SLC", and "Create secondary interferogram" processes. Two secondary

interferograms are shown in Figure 4. Now the process "Flatten secondary interferogram" is done. It will compute the phase due to topography from the unwrapped reference interferogram and subtract it from the secondary intereferogram. The two flattened secondary interferograms are shown in Figure 7. Next, filter and unwrap the flattened interferograms. The two unwrapped secondary interferograms are given in Figure 8. Then refine the baseline of the secondary interferogram. Figure 9 shows the two geometry-refined secondary inteferograms.

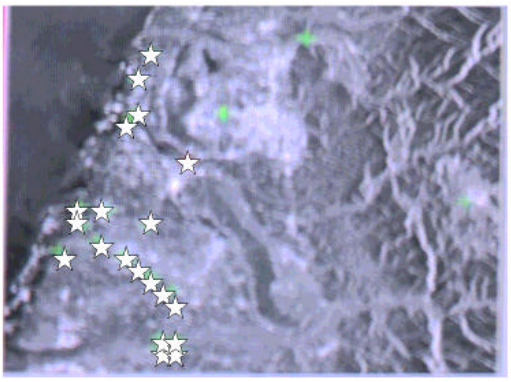

Figure 5. Distribution of GCPs where each star pattern denotes a GCP.

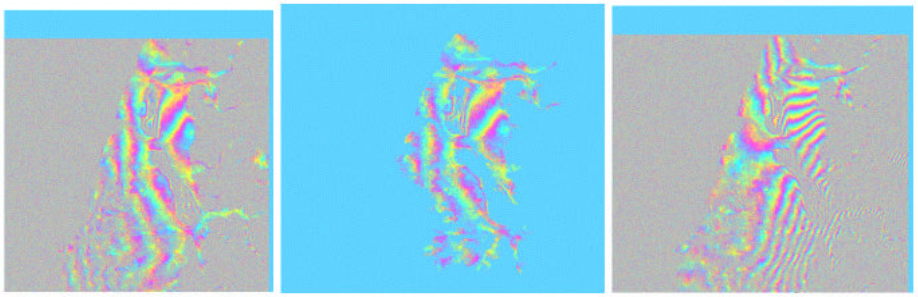

Figure 6. Filtered (left), unwrapped (middle), and geometry-refined (right) reference interferograms.

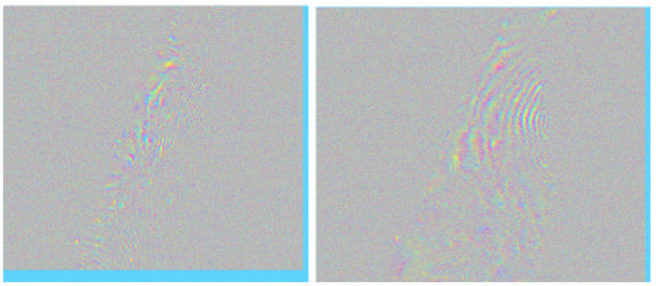

Figure 7. Two flattened secondary inteferograms: May 06/Sep. 23 (left), May 06/Oct. 28 (right).

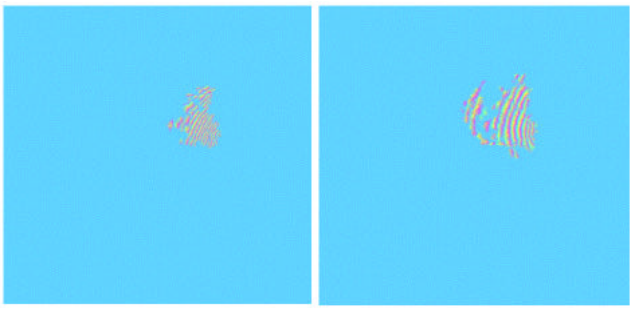

Figure 8. Two unwrapped secondary inteferograms: May 06/Sep. 23 (left), May 06/Oct. 28 (left).

In the last step, the displacement map will be generated. A digital displacement model (DDM) contains ground surface displacements, which are measured along the satellite look direction and are positive toward the satellite. Those values are then transformed into the local height datum system using the same way adopted in (Takeuchi et al., 2000). They are compared with the ones determined by GPS in fast static survey mode. On the left in Figure 10, we show the displacement map derived from the 1st set of May 06/Jan. 21/Sep. 23. It is displayed as a color image with a

wrap interval of 0.03meters. Its corresponding orthorectified power image is then shown on its right. In a same manner, the ones for the second set of May 06/Jan. 21/ Oct are also shown in Figure 10.

Figure 9. Two geometry-refined secondary inteferograms: May 06/Sep. 23 (left), May 06/Oct. 28 (right).

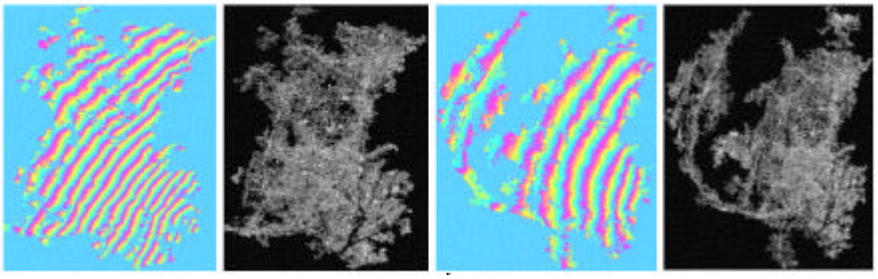

Figure 10. A color DDM image with a wrap interval of 3cm and its related orthorectified power image for the 1st set of May 06/Jan. 21/Sep. 23 and the 2nd set of May 06/Jan. 21/Oct. 28 (from left to right), respectively.

Comparing with 7 GPS-determined points shows that the mean difference of the displacement values estimated by D-INSAR and the ones determined by GPS is about 6.2cm and 6.5cm for the two sets, respectively. All differences have a absolute value of less than 18cm. It indicates that three-pass method and ERS data processed properly can detect height surface deformation in urban area in Taiwan.

6. CONCLUSION

Our preliminary test results show that the quality of the digital displacement model (DDM) determined using the three-pass method can reach at the accuracy level of centimeters, if all data are processed in a proper way. Ground control points (GCPs) are not used in regions where large displacements are observed. To improve the quality of the DDM determined by INSAR, *airborne* SAR might provide an applicable solution. Our main interests aim at the determination of a high precision DEM and/or DDM in those difficult regions for aerial photogrammetry, e.g. mountainous and dense vegetation areas in Taiwan. The details must be further studied in our future works.

7. REFERENCES

Curlander, J.C., and McDonough, R.N., 1991. Synthetic Aperture Radar – Systems and Signal Processing. John Wiley & Sons, New York, pp. 249-499.

Henderson, F.M., and Lewis, A.J., 1998. Principles and Applications of Imaging Radar. In: Manual of Remote Sensing, 3rd edition. John Wiley & Sons, New York, pp. 2-4.

Takeuchi, S.Y., Suga, Y., Oguro, Y., Chen, A.J., and Yonezawa, C., 2000. Verification of INSAR Capability for Disaster Monitoring – a Case Study on Chi-Chi earthquake in Taiwan. ACRS 2000, Vol. 2, pp. 738-743.

Tsay, J.-R., and Chen, H.-H., 2001. DEM generation in Taiwan by using INSAR and ERS data. To be presented in ACRS2001 (paper no. 104).

Vexcel, 2000. 3dSAR SAR Processing System, User's Manual.

Zebker, H.A., Rosen, P.A., Goldstein, R.M., Werner, C.L., and Gabriel, A., 1994. On the Derivation of Coseismic Displacement Fields Using Differential Radar Interfermetry: the Landers Earthquake. Journal of Geophysical Research, Vol. 99, No. B10, pp. 19617-19634.

Zebker, H.A., Rosen, P.A., and Hensley, S., 1997. Atmospheric effects in interferometric synthetic aperture radar surface deformation and topographic maps. Journal of Geophysical Research, Vol. 102, No. B4, pp. 7547-7563.

Zhou, Y.Q., Kless, R., Van Gendren, J.L., and Li, D.R., 1998. Differential SAR Interferometry: Priinciples and applications. Spatial Information Science Technology and its Applications, pp. 227-236.